https://doi.org/10.5194/egusphere-2024-2603
Preprint. Discussion started: 26 August 2024

Direct calibration using atmospheric particles and performance evaluation of PSM 2.0 for sub-10 nm particle measurements

Yiliang Liu[1,2], Arttu Yli-Kujala[2], Fabian Schmidt-Ott[2], Sebastian Holm[2], Lauri Ahonen[2], Tommy Chan[2], Joonas Enroth[3], Joonas Vanhanen[3], Runlong Cai[4], Tuukka Petäjä[2], Markku Kulmala[2], Yang Chen[1], and Juha Kangasluoma[2]

[1]Chongqing Institute of Green and Intelligent Technology, CAS, Chongqing, 400714, China
[2]Institute for Atmospheric and Earth System Research / Physics, University of Helsinki, Helsinki, 00014, Finland
[3]Airmodus Ltd., Helsinki, 00560, Finland
[4]Department of Environmental Science & Engineering, Fudan University, Shanghai, 200438, China

Correspondence to: Juha Kangasluoma (juha.kangasluoma@helsinki.fi), and Yang Chen (chenyang@cigit.ac.cn)

Abstract. Particle Size Magnifier is widely used for the measuring nano-sized particles. Here we calibrated the newly developed Particle Size Magnifier version 2.0 (PSM 2.0). 1-10 nm particles with different compositions were used, including metal particles, organic particles generated in the laboratory and atmospheric particles collected in Helsinki and Hyytiälä, respectively. Noticeable difference among the calibration curves was observed. Atmospheric particles from Hyytiälä required higher DEG supersaturation to be activated compared to metal particles (standard calibration particles) and other types of particles. This suggests that chemical composition differences introduce measurement uncertainties and highlight the importance of in-situ calibration. The size resolution of PSM 2.0 was characterized using metal particles. The maximum size resolution was observed at 2-3 nm. PSM 2.0 was then operated in Hyytiälä in parallel with a Half-mini Differential Mobility Particle Sizer (DMPS). During new particle formation (NPF) events, comparable total particle concentrations were observed between Half-mini DMPS and PSM 2.0 based on Hyytiälä atmospheric particle calibration. Meanwhile, applying the calibration with metal particles to atmospheric measurements would cause an overestimation of 3-10 nm particles. In terms of the particle size distributions, similar patterns were observed between DMPS and PSM when using the calibration of Hyytiälä atmospheric particles. In summary, PSM 2.0 is a powerful instrument for measuring sub-10 nm particles and can achieve more precise particle size distribution measurements with proper calibration.

1 Introduction

Particle Size Magnifier (PSM) is a powerful instrument for measuring the size distributions of nanoparticles. It finds extensive applications across various research domains, such as atmospheric studies (Kulmala et al., 2013; Winkler et al., 2008; Yao et al., 2018), nano material research (Liu et al., 2024; Wlasits et al., 2020), combustion research (Rönkkö et al., 2017), health sciences, etc. The prototype instrument was developed by Kogan et al. in 1960 (Kogan and Burnasheva, 1960), followed by a series of different types of designs (Kim et al., 2003; Okuyama et al., 1984; Sgro and Fernandez de la Mora, 2004). In 2011,

https://doi.org/10.5194/egusphere-2024-2603
Preprint. Discussion started: 26 August 2024

PSM version 1.0 was commercialized by Airmodus Ltd. (Vanhanen et al., 2011), and became available for research groups worldwide. In 2023, Airmodus Ltd. unveiled PSM version 2.0, boasting several enhancements over its predecessor (Sulo et al., 2024). These improvements include an expanded measurement size range, enhanced durability, higher instrument stability, and improved user-friendliness.

The activation of particles in PSM relies on heterogeneous nucleation under varying supersaturation of diethylene glycol (DEG) vapor. As DEG supersaturation increases, smaller particles become activated. The minimum particle size that can be activated is around 1 nm, at the brink of DEG homogeneous nucleation (Iida et al., 2011). However, the performance of PSM, as well as some other condensation-based instruments, is influenced by many factors. A review paper that summarizes and discusses the uncertainties is published recently (Kangasluoma et al., 2020). The uncertainties in particle activation come from the particle properties, ambient conditions, and instrument setups, etc. Environmental conditions such as humidity and air pressure can result in the offset between the DEG supersaturation and particle activation, and thereby introduce uncertainties for the measured particle size distributions (Liu et al., 2020). As the relative humidity (RH) of the carrier gas increases, nanoparticles can be activated at a lower DEG saturator flow rate, leading to a shift in the cut-off size towards smaller particles (Kangasluoma et al., 2013, 2016b). This phenomenon is attributed to the hygroscopic properties of nanoparticles and vapor-particle interactions due to hydrogen bonding (Keshavarz et al., 2020b; Toropainen et al., 2021). The charging state of particles also affects their activation. Charged particles tend to activate at a lower saturator flow rate compared to neutral particles (Kangasluoma et al., 2016a; Keshavarz et al., 2020a), because the charge on a particle reduces the energy barrier for DEG condensation.

Among all the influencing factors, the chemical composition of particles exerts the strongest influence on particle detection (Kulmala et al., 2007). Metal and salt particles typically exhibit higher detection efficiency by PSM compared to organic particles (Kangasluoma et al., 2014; Liu et al., 2022). The standard practice involves calibrating the PSM in a laboratory using metal particles and then employing it for measuring particles with complex and unknown compositions (Lehtipalo et al., 2021). This process inherently introduces some uncertainties due to the variation in chemical composition of particles used for calibration and measurement. Calibrating the PSM with particles of the same chemical composition as those being measured can minimize measurement uncertainties (Ahonen et al., 2017). However, applying this approach can be challenging, as it requires specific and directly relevant particle sources and a HR-DMA, which are not always readily available. Additionally, the measured nanoparticles often have complex compositions and low concentrations, making it difficult to generate particles with identical compositions in the laboratory.

In this study, we performed calibration on PSM 2.0 using different kinds of particles, including commonly-used metal particles, organic particles, as well as the direct calibration using atmospheric particles. In addition, PSM 2.0 was operated in parallel with a DMPS (Differential Mobility Particle Sizer) for the measurement of ambient particles. The results help us to have a better understanding about the effects of particle composition as well as the sizing accuracy of PSM 2.0.

https://doi.org/10.5194/egusphere-2024-2603
Preprint. Discussion started: 26 August 2024

2 Methods

2.1 Working principle of PSM 2.0

The working principle of PSM 2.0 is similar to that of its predecessor, PSM 1.0, involving a two-step activation and growth process for nanoparticles. First, particles are activated using supersaturated DEG vapor, where increased DEG supersaturation enables the activation of smaller particles. In the second step, the activated particles grow to an optically detectable size within a butanol-based CPC. The size distributions can be calculated through a proper data inversion process, and in this study the step inversion method was used (Cai et al., 2018b; Chan et al., 2020).

PSM 2.0 offers several improvements compared over PSM 1.0. Firstly, it features a more stable internal flow field, achieved by controlling DEG supersaturation through two distinct flows: a wet flow carrying DEG vapors and a dry flow of particle-free compressed air (Attoui et al., 2023). The wet flow rate can be adjusted between 0.05 and 1.90 L min^{-1}, while maintaining a stable total flow rate of wet and dry flows. The enhanced stability and precision in the flow system lead to more predictable dilution factors under different saturator flow rates and minimize concentration fluctuations caused by changing flow rates. Secondly, PSM 2.0 offers a broader range of DEG supersaturation adjustments than PSM 1.0. By controlling the ratio of dry to wet flow rates, it enables to achieve a lower supersaturation level, which is crucial for extending the instrument's size measurement range.

2.2 PSM 2.0 calibration

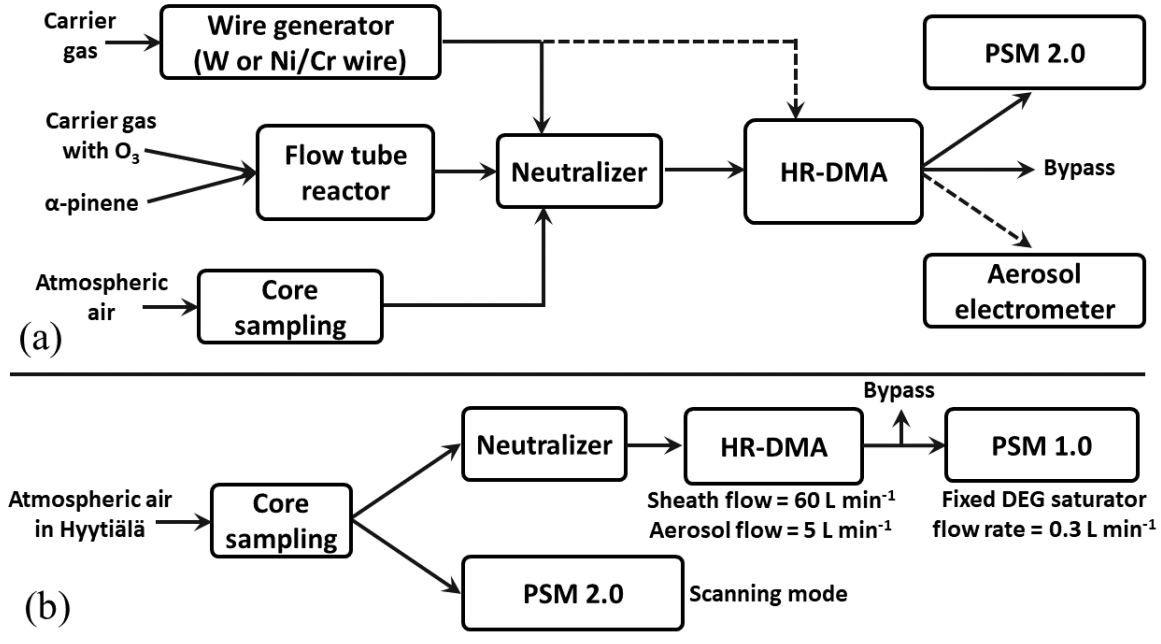

https://doi.org/10.5194/egusphere-2024-2603
Preprint. Discussion started: 26 August 2024

Figure 1. (a) A schematic diagram illustrating the calibration of PSM 2.0 using metal particles (tungsten and nickel/chromium particles), organic particles (alpha-pinene oxidation particles), and atmospheric particles collected in Helsinki and Hyytiälä. The flow configuration is detailed in Table 1. (b) PSM 2.0 operated in parallel with a DMPS to measure atmospheric particles in Hyytiälä. The HR-DMA operated with an aerosol flow rate of 5 L min^{-1} and a sheath flow rate of 60 L min^{-1}.

A schematic diagram for PSM 2.0 calibration is displayed in Fig. 1(a). Different types of particles were used, including tungsten metal particles, nickel/chromium particles, alpha-pinene oxidation particles, Helsinki atmospheric particles and Hyytiälä atmospheric particles (Table 1). Metal particles generated in wire generators are commonly used for PSM calibration, because they provide appropriate concentrations and their activation behaviour is similar to that of salt particles, which are assumed to be one of the major components of ambient aerosols (Kangasluoma et al., 2014, 2015). For the tungsten particle generation, nitrogen was used as the carrier gas, while synthesized air was used for Ni/Cr particle generation. Tungsten particles ranged in size from 1.2 to 20.3 nm across 68 sizes, whereas Ni/Cr particles ranged from 1.2 to 14.0 nm across 10 sizes. Organic particles were generated in the flow tube reactor through the reaction of alpha-pinene with ozone. The generation method was comparable to that mentioned in a previous study (Li et al., 2022). The particles, ranging in size from 1.6 to 9.4 nm, were classified into 10 sizes and used for PSM 2.0 calibration.

We also used atmospheric particles for PSM 2.0 calibration. Burst increase of sub-10 nm particle concentrations was observed during NPF events in Helsinki and Hyytiälä. The standard temperature settings by the manufacturer were used for all calibration experiments, and one more calibration was performed under boosted temperature setting in Hyytiälä. The temperatures for both the standard and boosted settings are displayed in Table 2.

After the particle generation, the aerosol flow passed through a neutralizer (Ni-63) before undergoing size classification by an HR-DMA (Cai et al., 2018a; Fernandez de la Mora, 2017). Some of the metal particles were self-charged, so the neutralizer was removed when using sub-3 nm tungsten to calibrate the instrument. It will help to eliminate the effects of neutralizer ions of the calibration. High sheath flow rates were generally used for classifying metal particles to enhance their monodispersity in the laboratory experiments. Conversely, a lower DMA sheath flow rate (60 L min^{-1}) was used for the classification of atmospheric particles to increase their concentration signal.

After the HR-DMA classification, the monodispersed particles were directed to PSM 2.0 and an Aerosol Electrometer (AEM) at equal flow rates of 2.7 L min^{-1}. PSM 2.0 was operated in scanning mode, with the DEG saturator flow rate(s) repeatedly increasing and decreasing between 0.05 and the peak value (usually 1.9 L min^{-1}). Particle concentrations at different DEG saturator flow rates were recorded. The AEM was only used for the calibration using metal particles. For the calibration using atmospheric particles, the particle concentrations after the DMA classification were very low (<100 cm^{-3}). The identification of true particle concentrations without AEM is based on the plateau concentrations by PSM 2.0 at high DEG saturator flow rates.

Table 1. Summary of particles used for PSM 2.0 calibration. The particles were either generated in the laboratory using particle generators or sampled from atmosphere during NPF events.

https://doi.org/10.5194/egusphere-2024-2603
Preprint. Discussion started: 26 August 2024

#	Particle source	Particle type	Carrier gas	Neutralizer	HR-DMA sheath flow (L min^{-1})	HR-DMA aerosol flow (L min^{-1})	Particle size range (nm)	Aerosol electrometer
1	Wire generator	Tungsten particles	N_2	√	300, 145, 100	10	1.2-20.3	√
2	Wire generator	Nickel/chromium particles	Synthesized air	√	200	10	1.2-14.0	√
3	Organic particle generator	Alpha-pinene oxidation particles	Synthesized air	√	150	5.4	1.6-9.4	√
4	Helsinki ambient air	Ambient particles	Atmospheric air	√	60	5	2-11	
5	Hyytiälä ambient air	Ambient particles	Atmospheric air	√	60	5	2.5-11	

2.3 Campaign measurement

After the calibration, PSM 2.0 was operated in parallel with a DMPS to measure ambient particles in Hyytiälä (Fig. 1(b)). This lasted for three weeks from 1 May to 21 May, 2024. The instrument configurations are displayed in Table 2. Both the PSM 2.0 and DMPS used core-sampling method, with a carrier gas flow rate of 10.0 L min^{-1} in the main sampling tube. PSM 2.0 was operated under the scanning mode, with the DEG saturator flow rate increasing from 0.05 to 1.80 L min^{-1}, and then decreasing. Each DEG scan took 4 minutes. A step inversion method was used for PSM 2.0 data inversion, based on calibrations using different types of particles.

Table 2. Configuration settings for PSM 2.0 and DMPS during the ambient particle measurement in Hyytiälä.

Instrument	Core sampling	Neutralizer	Mode	Setting	Time per scan	Size bins
PSM 2.0	√		DEG scanning from 0.05 to 1.80 L min^{-1}	Inlet/saturator/condenser = 40/71/10 (°C) *	240 s	6-9
DMPS	√	√	Voltage scanning from 100 to 2000 V	Sheath/aerosol = 60:5(L min^{-1})	220 s	10

* Under the boosted PSM temperature setting, the temperature of the condenser was 7 °C.

For DMPS (Kangasluoma et al., 2018), after the core-sampling, aerosol flow passed through a Ni-63 neutralizer at a flow rate of 5.0 L min^{-1}. Particles were then size-classified by a half-mini DMA (sheath flow rate of 60 L min^{-1}). PSM 1.0 was used as the concentration detector of DMPS, which operated at a fixed DEG saturator flow rate of 0.3 L min^{-1} (with a background concentration of almost 0 cm^{-3}). We used the inversion method as displayed in a previous study (Jiang et al., 2011). An equivalent length of 1.8 m was used to correct the diffusion losses inside the neutralizer. A charging steady state was assumed

https://doi.org/10.5194/egusphere-2024-2603
Preprint. Discussion started: 26 August 2024

to be achieved inside the neutralizer (Wiedensohler and Fissan, 1991). The transmission function of half-mini DMA was obtained from a previous study (Cai et al., 2018b). The detection efficiencies of different sized particles by the PSM 1.0 were calibrated using alpha-pinene oxidation particles.

2.4 Data processing

2.4.1 Detection efficiency curve

For particles of a certain size, their detection efficiencies (η) at different DEG saturator flow rates were calculated based on the ratios of the concentrations measured by PSM 2.0 and actual concentrations. For metal particles, the actual concentrations were typically higher than 1000 cm^{-3}, and could be measured by the AEM. However, in terms of ambient particles after DMA classification, their concentrations were identified based on the assumption that a stable plateau observed under high DEG saturator flow rates represented the real particle concentrations. The detection efficiencies under different DEG saturator flow rates were fitted using the following Eq. (1):

$$\eta = \frac{1}{\left(1+e^{(-a\cdot(s-b))}\right)}, \quad (1)$$

where s is the DEG saturator flow rate, a and b are fitting parameters.

2.4.2 Kernel function curve

The Kernel function represents the derivative of the fitted detection efficiency curve with respect to the saturator flow rate (Cai et al., 2018b). The peak point of the Kernel function helps to establish the correlation between the DEG saturator flow rates and the cut-off sizes. Additionally, the width of the Kernel function suggests if the activation of particles happened within a narrow DEG saturator flowrate variation or a wide range. The sizing resolution in DEG saturator flow rate space ($Res(S^*)$) of PSM 2.0 can be evaluated, accordingly:

$$Res(S^*) = \frac{S^*}{\Delta S} \quad (2)$$

where S^* is the saturator flow rate corresponding to the peak point of the Kernel function, and ΔS is the full width at half maximum of the Kernel function peak.

Several factors influence $Res(S^*)$, including the temperature configuration of the PSM, the uniformity and stability of DEG supersaturation within the instrument, and the uniformity of the size and chemical composition of the particles (Fernandez de la Mora et al., 2022). Meanwhile, the incomplete detection efficiency curves and Kernel functions would introduce some uncertainties in the calculated $Res(S^*)$. Generally, increasing the temperature difference between the PSM's saturator and condenser results in a dramatic change in supersaturation, thereby enhancing the $Res(S^*)$. Conversely, variations in particle composition and poor monodispersity of particles can broaden the measured kernel function peaks, leading to a decrease in $Res(S^*)$. This study did not attempt to quantify the impact of these factors. Instead, we used the standard temperature settings by Airmodus and characterized PSM 2.0's $Res(S^*)$ using metal particles.

https://doi.org/10.5194/egusphere-2024-2603
Preprint. Discussion started: 26 August 2024

However, the $Res(S^*)$ alone cannot demonstrate the sizing capability of the PSM 2.0, because the relationship between particle sizes and DEG saturator flow rates is not linear. In terms of metal particles, slight variations in the saturator flow rate would lead to significant fluctuations in the corresponding cut-off sizes (Fig. 5). To address this, we cited the DMA's definition of size resolution, by replacing the DEG saturator flow rate in the Kernel function with the corresponding cut-off size (based on the calibration curve). After that, we calculated the size resolution of PSM ($Res(d_p^*)$) at specific particle size (d_p^*):

$$Res(d_p^*) = {d_p^*}/{\Delta d_p} = Res(S^*)\frac{d_p^*}{S^*}\frac{1}{-f'[S^*]}, \quad (3)$$

where $f[S^*]$ is the fitted function displaying the cut-off size at the saturator flow rate of S^*. $f'[S^*]$ suggests the derivation of the fitted function at the DEG saturator flow rate of S^*. In general, the size resolution of PSM is related to the DEG resolution, and also the calibration curve. Please refer to SI for the detailed derivation process.

2.4.3 Calibration curve

The calibration curve was based on the peak points of different-sized particles in the Kernel functions, and showed a one-to-one correspondence between the DEG saturator flow rate and cut-off size. Various types of particles were used to calibrate the PSM 2.0, resulting in different calibration curves. This relationship is crucial for PSM 2.0 data inversion. In terms of the step inversion method, the activation of particles larger than the cut-off size are assumed to be 100%, while for particles smaller than the cut-off size, their activation efficiencies are assumed to be 0%.

3 Results and discussion

3.1 PSM 2.0 Calibration using metal particles

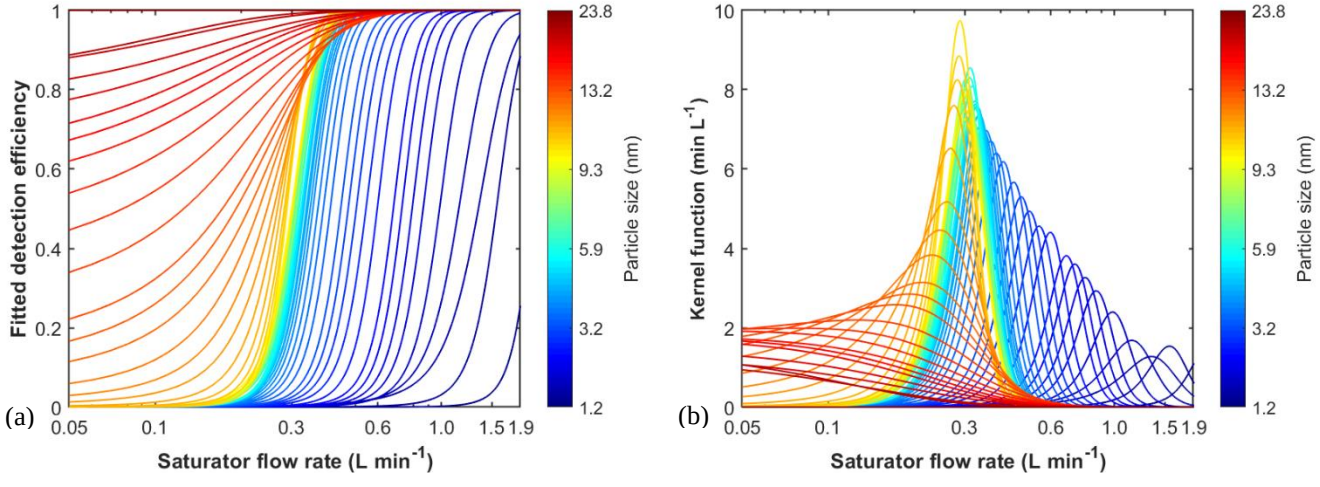

Figure 2. (a) The fitted detection efficiency curves according to the calibration using tungsten particles. (b) The calculated Kernel function curves according to the fitted detection efficiencies curves.

https://doi.org/10.5194/egusphere-2024-2603
Preprint. Discussion started: 26 August 2024

Figure 2(a) presents the detection efficiency curves for different sized tungsten particles. The detection efficiency curves can be divided into two groups. The first group is for sub-10 nm particles, where the fitted detection efficiency curves maintain a consistent and approximate parallel pattern. As particle size increase, a leftward shift in the detection efficiency curve is observed. The detection efficiency increasing from 0% to plateau values (close to 100%) can be found as the DEG saturator flow rate increasing. Plateau values close to 100% were observed because the dilution factor under different DEG saturator flow rates were well calibrated in the PSM 2.0. The second group is for particles larger than 10 nm, where the detection efficiency curves start to flatten out, with increased detection efficiencies observed at the lowest saturator flow rate (0.05 L min^{-1}). This is because the activation of particles larger than 10 nm started to be influenced by the activation in the down-stream CPC.

Due to variations in detection efficiency curves for particles of varying sizes, PSM 2.0 can theoretically detect particles ranging from 1 to 20 nm. However, calibrating particles within the 10-20 nm range yields higher uncertainties. Concentrations measured by the AEM were gradually higher than PSM 2.0, as particle size closing to 20 nm. This discrepancy probably arises from the multiply charged particles, leading to overestimation in concentrations by AEM. Consequently, the concentrations measured by PSM 2.0 at the high DEG flow rates were adopted as the actual particle concentrations and used to plot the detection efficiency curves.

$Res(S^*)$ of PSM 2.0 remained stable for particle sizes 2.0 to 10.0 nm, approximately 3 (Fig. 3). The decreasing trend in the resolution for sub-2 nm particles may come from the changes in chemical compositions within this size range. To get a high concentration of sub-2 nm particles for instrument calibration, a higher heating power was used by the wire generator, which could possibly increase the fraction of organic components in nanoparticles. For particles larger than 10 nm, we observed a decrease in the $Res(S^*)$. For sub-3 nm particles, the $Res(S^*)$ of PSM 2.0 were quite comparable with PSM 1.0 (Cai et al., 2018b). In 3 to 4 nm size range, a decrease in the $Res(S^*)$ can be found for PSM 1.0, whereas for PSM 2.0, the $Res(S^*)$ remained stable till 10 nm. PSM 2.0 showed a higher $Res(S^*)$ than PSM 1.0 possibly because PSM 2.0 ensures a more stable flow field and enables more precise and uniform control over DEG supersaturation.

https://doi.org/10.5194/egusphere-2024-2603
Preprint. Discussion started: 26 August 2024

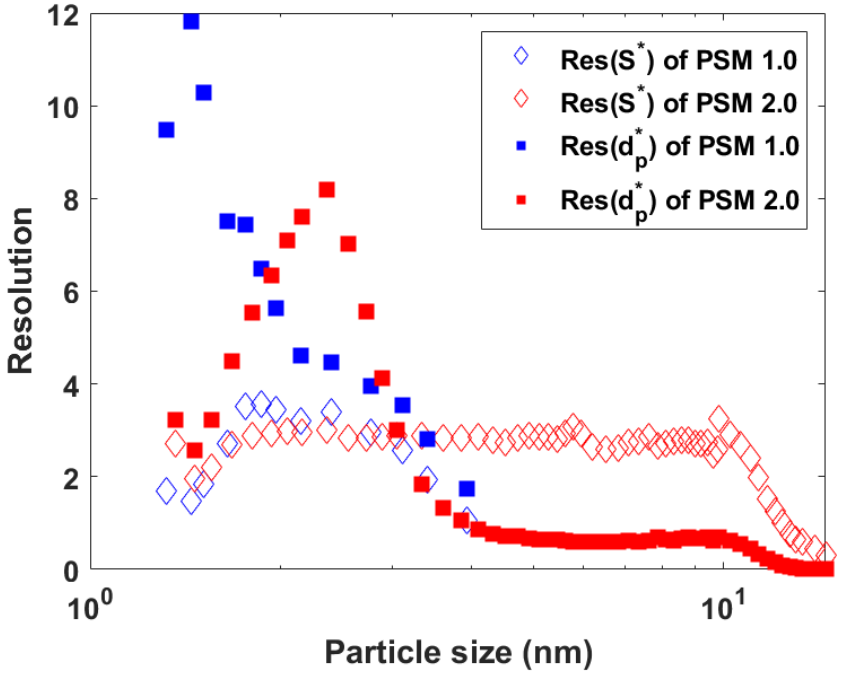

Figure 3. Resolution in DEG saturator flow rate ($Res(S^*)$) and size resolution ($Res(d_p^*)$) for both PSM 2.0 and PSM 1.0. The calculations are based on metal particles classified by an HR-DMA. Commercial temperature settings were used for both instruments. The $Res(S^*)$ of PSM 1.0 are cited from Cai et al. (2018a).

The size resolution ($Res(d_p^*)$) of PSM 2.0 were also compared with PSM 1.0. For PSM 1.0, a decreasing trend in size resolution was observed as particle size increased. For PSM 2.0, the peak size resolution was observed at around 2.2 nm. As mentioned above, the decrease in size resolution for particles smaller than 2.2 nm is similar to the decrease in DEG resolution, as metal particles produced in the wire generator were contaminated by more organic impurities. For particles larger than 4 nm, the size resolution of PSM 2.0 was stable but was lower than 1. In summary, though PSM 2.0 expanded the size measurement range from 4 nm of PSM 1.0 to above 10 nm, but the size resolution on 4-10 nm particles was low (<1). For particles larger than 10 nm, the size resolution further decreased, indicating larger sizing uncertainties.

https://doi.org/10.5194/egusphere-2024-2603
Preprint. Discussion started: 26 August 2024

3.2 PSM 2.0 calibration with ambient particles

3.2.1 Ambient particles in Helsinki

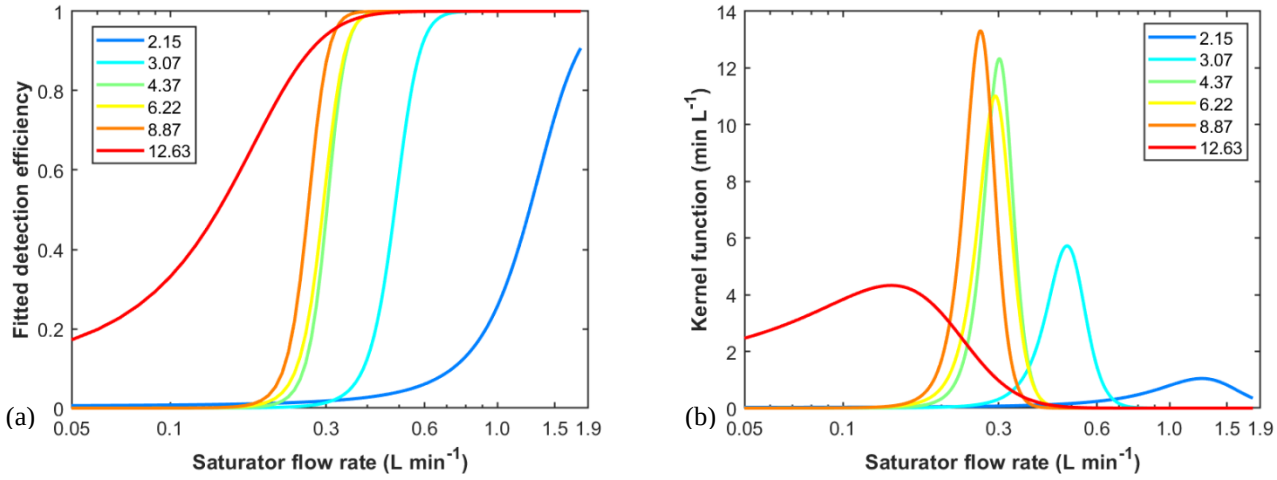

Figure 4. PSM 2.0 calibration based on the ambient particles collected in Helsinki during an NPF event on 18 February. (a) Detection efficiency curves of different sized particles. (b) Kernel function curves of different sized particles.

Two NPF events in Helsinki were identified on 18 and 19 February, respectively. The size-resolved detection efficiency curves are displayed in Fig. 4 (a). In general, for particles larger than 3 nm, the detection efficiency curves can be well fitted, because a plateau value in the detection efficiency curve can be well identified. However, for sub-3 nm particles, especially for sub-2 nm particles, the particles' concentrations were low. Therefore, only particles larger than 2 nm were used for plotting the PSM 2.0 calibration curves. The detection efficiency curves moved toward left side, as particles' size increased. The Kernel function was also plotted (Fig. 4 (b)).

We further compared the calibration results for different types of particles (Fig. 5). Overall, the calibration curves of metal particles, by using tungsten and Ni/Cr particles, are comparable. For organic particles, the activation of sub-4 nm particles needs higher DEG saturator flow rate compared to metals. However, for particles larger than 4 nm, the activation is slightly lower than metal particles.

For atmospheric particles sized between 2-4 nm, the activation of Helsinki ambient particles required a slightly higher DEG saturator flow rate than for metal particles. Whereas opposite trend was observed for particles larger than 4 nm, which could be related to the higher RH in the ambient atmosphere. Our experiments confirmed the validity of using metal particles for calibration, and subsequently using the PSM 2.0 to measure atmospheric particles in Helsinki. However, the composition of ambient particles can vary significantly between different cities, as the sources of nucleation mode particles and the mechanisms of new particle formation (NPF) can differ.

https://doi.org/10.5194/egusphere-2024-2603
Preprint. Discussion started: 26 August 2024

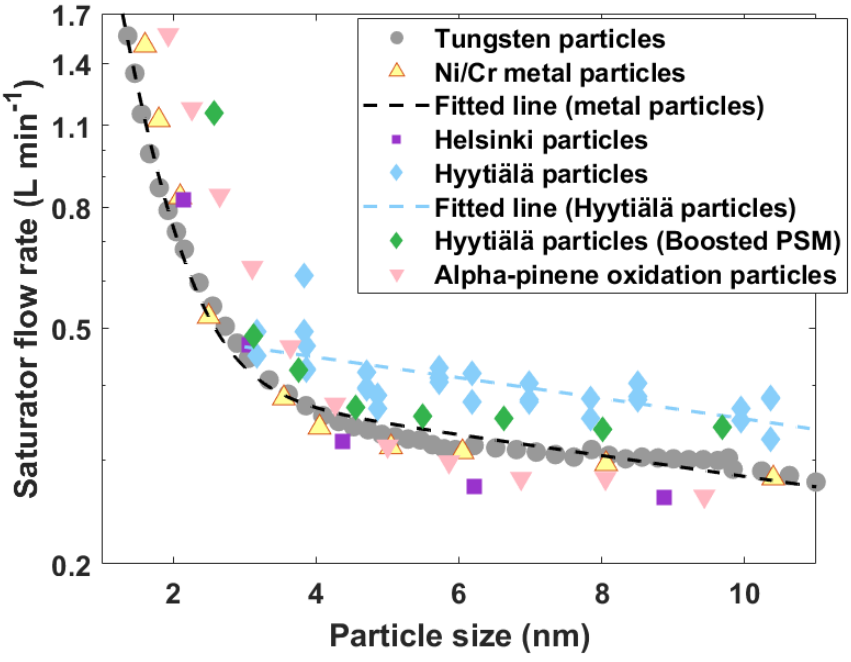

Figure 5. The relationship between DEG saturator flow rates and the corresponding cut-off sizes. The calibrations curves were plotted based on different types of particles, including metal particles, organic particles, and ambient particles collected in different places.

3.2.2 Ambient particles in Hyytiälä

A total of 6 NPF events were identified in Hyytiälä, on 5, 6, 10, 11, 12 March and 4 April, respectively. Among these, 5 events were used to calibrate PSM 2.0 under standard temperature settings, except the event on 4 April, that was used to calibrate the boosted PSM 2.0, with the condenser temperature of 7°C. The fitted detection efficiency curves based on different-sized particles are given in the SI. Only the result of particles larger than 3 nm was used for plotting the calibration curve (Fig. 5), due to the low concentrations of sub-3 nm particles.

Notably, a higher saturator flow rate was needed for the activation of Hyytiälä ambient particles, compared with metal particles, organic particles, or the ambient particles in Helsinki. It suggests the composition difference between Hyytiälä ambient particles and other types of particles, which would cause the difference in their activation in PSM 2.0. The ambient particles in Hyytiälä predominantly comprised of organic components, but is different from the alpha-pinene oxidation particles generated in the lab. This observation was further corroborated by the boosted PSM 2.0 experiment. By increasing the temperature difference between the saturator and condenser, the calibration curve moves toward to the calibration curve of metal particles.

https://doi.org/10.5194/egusphere-2024-2603
Preprint. Discussion started: 26 August 2024

3.3 Ambient particle size distribution measurement

We used 4 NPF events in Hyytiälä that happened between 8 and 11 May, and compared the particle size distributions inverted using different calibrations. Subsequently, these inverted size distributions were compared with the DMPS.

3.3.1 Total concentrations of 3-10 nm particles

Three calibration curves based on tungsten particles, Helsinki atmospheric particles, and Hyytiälä atmospheric particles are used for the data inversion. The upper size limit for all three calibrations exceeds 10 nm. Obviously, PSM 2.0 is capable for the measurement of particles close to 1 nm, as displayed in the result of metal particles (Fig. 5). However, there was a lack of signal intensity when performing the calibration using ambient particles. As displayed in Fig. S1-S3, under the condition of low sub-3 nm particle concentrations, it is hard to identify the presence of plateau concentrations as well as fitting the detection efficiency curves. As a result, the lower size limits differ for different calibrations: for metal particles, the calibration is performed down to 1 nm, while for Helsinki and Hyytiälä particles, the smallest detectable sizes were around 2 and 3 nm, respectively. To compare the total concentrations, we selected a common measurement size range of 3-10 nm (Fig. 6).

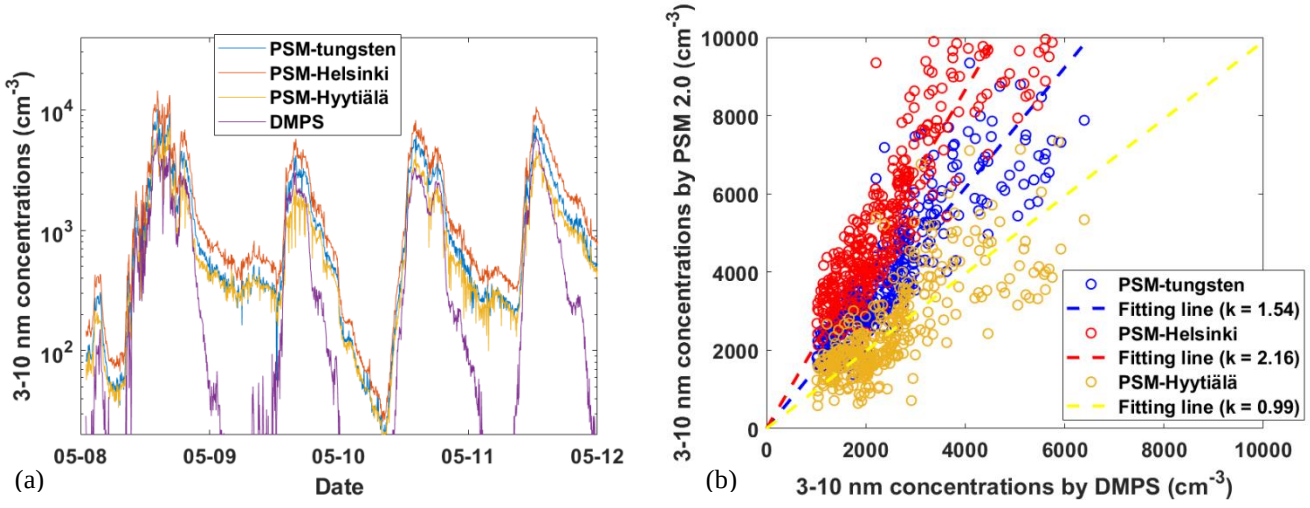

Figure 6. (a) 3-10 nm particle concentrations by PSM 2.0 and DMPS. Different types of particles were used for PSM 2.0 data inversion. (b) Comparison of total concentrations (sized between 3.1 to 10.1 nm) measured by DMPS and PSM 2.0 using different calibration methods. Only the DMPS total concentration results exceeding 1000 cm^{-3} are shown. The fitting line is based on the scattered data. A good correlation between PSM 2.0 and DMPS was observed, when Hyytiälä atmospheric particles was used for PSM 2.0 calibration.

During the NPF events, high concentrations of 3-10 nm particles were observed. The concentrations of 3-10 nm particles measured by PSM 2.0 and DMPS were displayed in Fig. 6(a). The total concentrations measured by PSM and DMPS were scattered, when the total concentrations measured by DMPS were higher than 1000 cm^{-3} (Fig. 6(b)). The best alignment between DMPS and PSM 2.0 measurements occurred when using the Hyytiälä atmospheric particle calibration, showing a slope close to 1 in the linear regression analysis. In contrast, the other two calibration files resulted in overestimations of 1.54

https://doi.org/10.5194/egusphere-2024-2603
Preprint. Discussion started: 26 August 2024

and 2.16, respectively. This suggests that the calibration significantly influences the discrepancy in particle concentration between PSM and DMPS measurements.

However, during non-NPF events, when total concentrations were lower than 1000 cm^{-3}, the concentrations measured by DMPS were significantly lower than those measured by PSM 2.0. This is because PSM is more suitable for measuring low concentrations of nanoparticles. DMPS tends to underestimate concentrations, particularly as particle size decreases. This underestimation occurs because the penetration efficiency of nanoparticles in the DMPS is significantly affected by the processes of charging, classification, transport, and detection. Consequently, the concentrations measured by DMPS are often underestimated.

3.3.2 Particle number size distributions measured by PSM 2.0

The inverted particle number size distributions by PSM 2.0 were determined by the calibration file. Calibration of PSM 2.0 using atmospheric particles from Hyytiälä was limited to a minimum size of 3 nm. We selected the common size range across two instruments, and conducted an intercomparison. The overall size distributions measured by PSM 2.0 and DMPS were displayed in Fig. 7. Significant differences were observed when different calibrations being used. DMPS showed similar pattern in 3-10 nm with the PSM 2.0 by using the calibration obtained with Hyytiälä atmospheric particles. In contrast, the calibration based on tungsten and Helsinki atmospheric particles revealed an opposite trend.

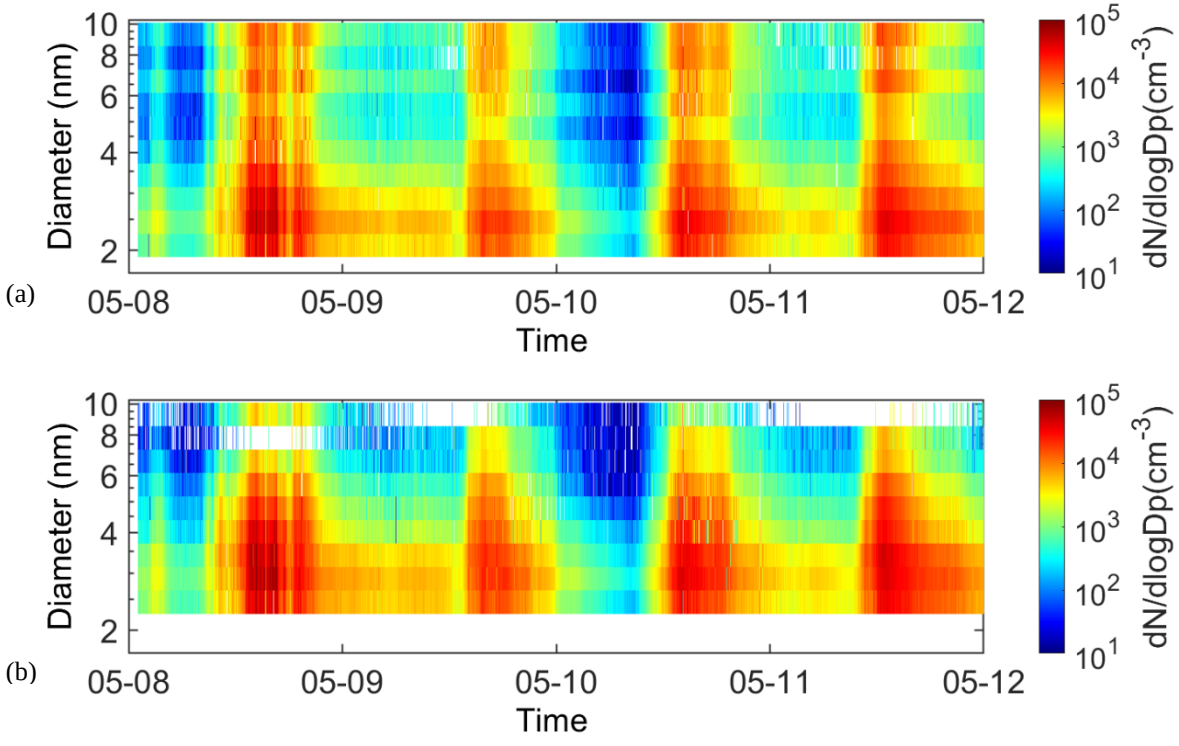

https://doi.org/10.5194/egusphere-2024-2603
Preprint. Discussion started: 26 August 2024

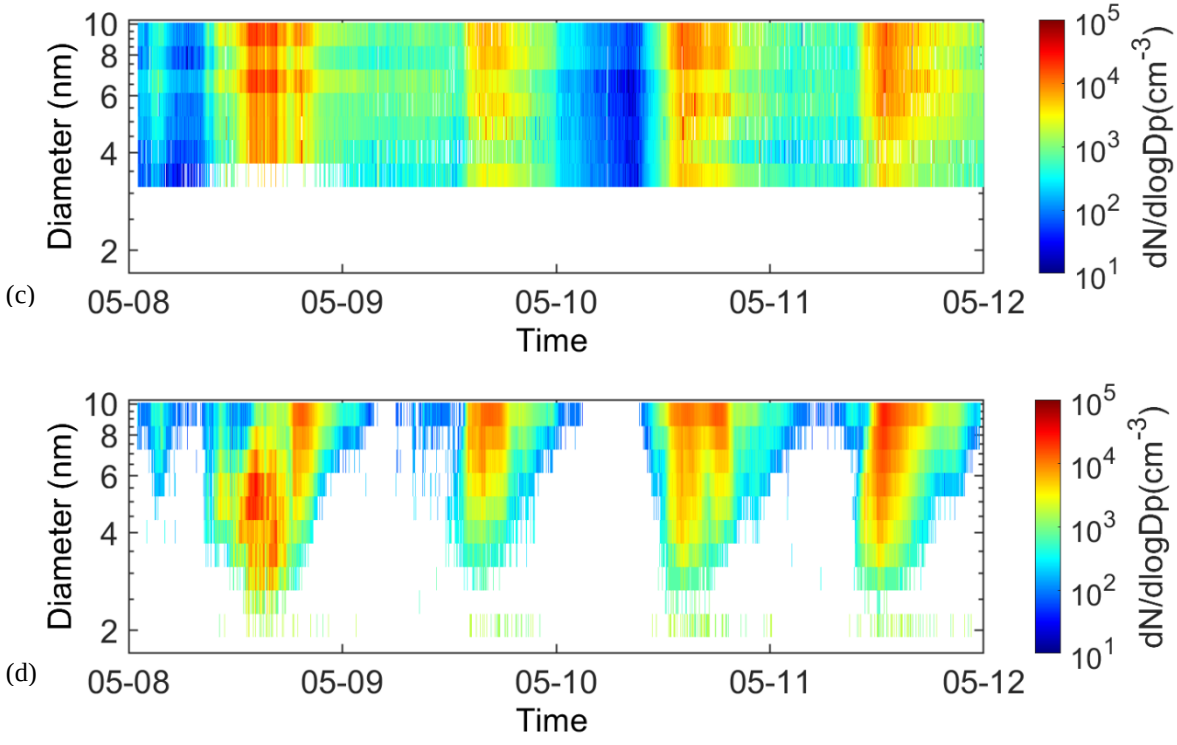

Figure 7. (a) Number size distributions measured by PSM 2.0 using the calibration of tungsten particles. (b) Number size distributions measured by PSM 2.0 using the calibration of Helsinki ambient particles. (c) Number size distributions measured by PSM 2.0 using the calibration of Hyytiälä ambient particles. (d) Number size distributions measured by DMPS.

To enhance the clarity of the intercomparison, we compared the mean number size distributions measured during four NPF events (from 13:00 to 15:00) (Fig. 8). Our result suggests that the inverted particle size distributions are sensitive to the calibrations. In the sub-3 nm size range, PSM 2.0 measurements using the calibration for tungsten particles and Helsinki ambient particles exhibited higher concentrations compared to DMPS results. As displayed in Fig. 5, the Hyytiälä atmospheric particles would need a higher DEG saturator flow rate to be activated. By using the wrong calibration file, the ambient particles larger than 3 nm were wrongly attributed to sub-3 nm size range, which caused the overestimation of sub-3 nm particles.

In four NPF events, three events (from 9 to 11 May) exhibited a similar particle size distribution pattern between DMPS and PSM 2.0 using the Hyytiälä atmospheric particle calibration, except for the event on 8 May. During that event, DMPS showed a peak concentration between 4-6 nm, with a noticeable decrease in concentration as particle size increased. Due to PSM 2.0's lower size resolution in this range compared to DMPS, the measured particle size distribution tended to flatten out.

We do not assert that the results displayed by DMPS are absolutely accurate, as DMPS itself is subject to inherent uncertainties. However, within the size range of 3-10 nm, DMPS (and SMPS) is the most widely used instrument, and its sizing is more reliable. Meanwhile, PSM 2.0 can provide comparable particle size distribution in this size range. Considering PSM 2.0 and DMPS are based on different working principles, this consistency is noteworthy.

https://doi.org/10.5194/egusphere-2024-2603
Preprint. Discussion started: 26 August 2024

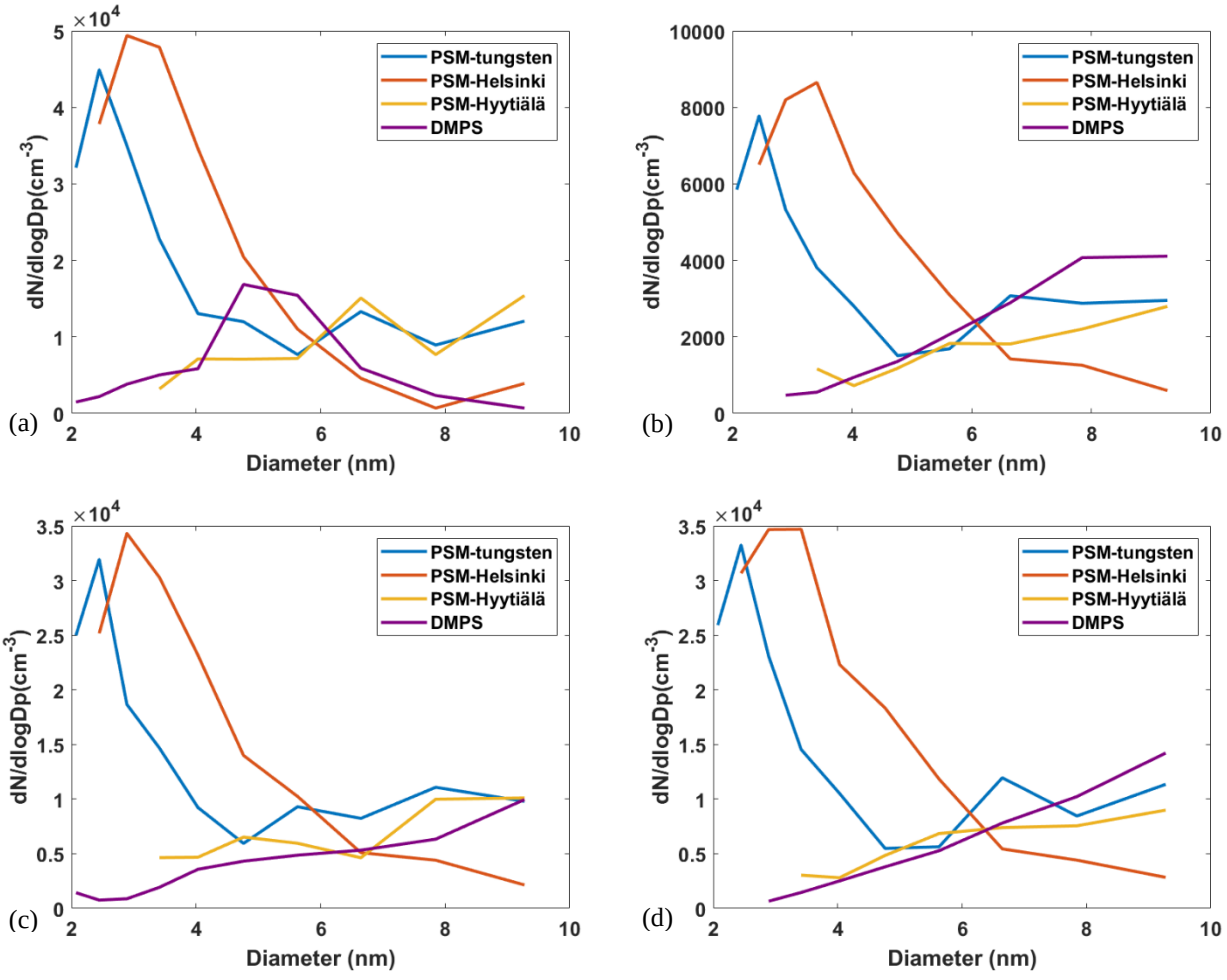

Figure 8. Mean number size distributions measured by PSM 2.0 and DMPS. The calibration of PSM 2.0 was based on tungsten metal particles, Helsinki atmospheric particles, and Hyytiälä atmospheric particles, respectively. The size distributions were collected during NPF events that occurred (a) from 13:00 to 15:00 on 8 May, (b) from 13:00 to 15:00 on 9 May, (c) from 13:00 to 15:00 on 10 May, and (d) from 13:00 to 15:00 on 11 May.

4. Conclusions

In this study, we calibrated the PSM 2.0 using different types of particles including tungsten particles, Ni/Cr particles, alpha-pinene oxidation particles, and atmospheric particles from Helsinki and Hyytiälä, respectively. Number size distributions of sub-10 nm particles based on different calibrations were investigated and compared with those measured by a DMPS. Calibration with Helsinki ambient particles showed a similar trend to metal particles, possibly because the composition of urban particles has the similar activation behaviour with metal particles. However, the activation of Hyytiälä ambient particles required higher DEG saturator flow rates. This difference underscores the significance of particle composition in calibration

https://doi.org/10.5194/egusphere-2024-2603
Preprint. Discussion started: 26 August 2024

processes. Proper calibration enables PSM 2.0 to enhance its reliability. After in-situ calibration (using Hyytiälä atmospheric particles), PSM 2.0 exhibited a good correlation with DMPS in terms of both total concentrations and particle size distributions, particularly during NPF events. However, using a wrong calibration will lead to deviations in the inversion results. PSM 2.0 also showed its effectiveness in measuring low concentrations of sub-10 nm particles. This study did not perform in-situ PSM 2.0 calibration using particles close to 1 nm due to the NPF events not being strong enough. Such calibrations are expected in the future to further reduce the measurement uncertainty of PSM 2.0.

Code/Data availability

The characterizations of the tested PSM 2.0 are shown in the figures. The codes for the inversion methods are available upon request.

Author contribution

JK and YL designed the experiments. YL, AY, FS, and LA carried them out. YL prepared the manuscript with contributions from all co-authors.

Competing interests

The authors declare that they have no conflict of interest.

Disclaimer

Publisher's note: Copernicus Publications remains neutral with regard to jurisdictional claims made in the text, published maps, institutional affiliations, or any other geographical representation in this paper. While Copernicus Publications makes every effort to include appropriate place names, the final responsibility lies with the authors

Acknowledgements

This work was funded by the Chongqing Natural Science Foundation (CSTB2022NSCQ-MSX1518), and the Research Council of Finland (356134, 346370, 364223).

https://doi.org/10.5194/egusphere-2024-2603
Preprint. Discussion started: 26 August 2024

References

Ahonen, L. R., Kangasluoma, J., Lammi, J., Lehtipalo, K., Hämeri, K., Petäjä, T., and Kulmala, M.: First measurements of the number size distribution of 1–2 nm aerosol particles released from manufacturing processes in a cleanroom environment, Aerosol Sci. Technol., 51, 685–693, https://doi.org/10.1080/02786826.2017.1292347, 2017.

Attoui, M., Perez-Lorenzo, L. J., Brock, C. A., and Fernandez de la Mora, J.: High resolution characterization of a sheathed axisymmetric variable supersaturation condensation particle sizer, J. Aerosol Sci., 169, 106112, https://doi.org/10.1016/j.jaerosci.2022.106112, 2023.

Cai, R., Attoui, M., Jiang, J., Korhonen, F., Hao, J., Petäjä, T., and Kangasluoma, J.: Characterization of a high-resolution supercritical differential mobility analyzer at reduced flow rates, Aerosol Sci. Technol., 52, 1332–1343, https://doi.org/10.1080/02786826.2018.1520964, 2018a.

Cai, R., Yang, D., Ahonen, L. R., Shi, L., Korhonen, F., Ma, Y., Hao, J., Petäjä, T., Zheng, J., Kangasluoma, J., and Jiang, J.: Data inversion methods to determine sub-3 nm aerosol size distributions using the particle size magnifier, Atmos. Meas. Tech., 11, 4477–4491, https://doi.org/10.5194/amt-11-4477-2018, 2018b.

Chan, T., Cai, R., Ahonen, L. R., Liu, Y., Zhou, Y., Vanhanen, J., Dada, L., Chao, Y., Liu, Y., Wang, L., Kulmala, M., and Kangasluoma, J.: Assessment of particle size magnifier inversion methods to obtain the particle size distribution from atmospheric measurements, Atmos. Meas. Tech., 13, 4885–4898, https://doi.org/10.5194/amt-13-4885-2020, 2020.

Fernandez de la Mora, J.: Expanded flow rate range of high-resolution nanoDMAs via improved sample flow injection at the aerosol inlet slit, J. Aerosol Sci., 113, 265–275, https://doi.org/10.1016/j.jaerosci.2017.07.020, 2017.

Fernandez de la Mora, J.: Size resolution of the Airmodus A10 particle size magnifier with purified clusters, J. Aerosol Sci., 160, 105916, https://doi.org/10.1016/j.jaerosci.2021.105916, 2022.

Iida, K., Stolzenburg, M. R., and McMurry, P. H.: Effect of Working Fluid on Sub-2 nm Particle Detection with a Laminar Flow Ultrafine Condensation Particle Counter, Aerosol Sci. Technol., 43, 81–96, https://doi.org/10.1080/02786820802488194, 2011.

Jiang, J., Chen, M., Kuang, C., Attoui, M., and McMurry, P. H.: Electrical Mobility Spectrometer Using a Diethylene Glycol Condensation Particle Counter for Measurement of Aerosol Size Distributions Down to 1 nm, Aerosol Sci. Technol., 45, 510–521, https://doi.org/10.1080/02786826.2010.547538, 2011.

Kangasluoma, J., Junninen, H., Lehtipalo, K., Mikkilä, J., Vanhanen, J., Attoui, M., Sipilä, M., Worsnop, D., Kulmala, M., and Petäjä, T.: Remarks on Ion Generation for CPC Detection Efficiency Studies in Sub-3-nm Size Range, Aerosol Sci. Technol., 47, 556–563, https://doi.org/10.1080/02786826.2013.773393, 2013.

Kangasluoma, J., Kuang, C., Wimmer, D., Rissanen, M. P., Lehtipalo, K., Ehn, M., Worsnop, D. R., Wang, J., Kulmala, M., and Petäjä, T.: Sub-3 nm particle size and composition dependent response of a nano-CPC battery, Atmos. Meas. Tech., 7, 689–700, https://doi.org/10.5194/amt-7-689-2014, 2014.

https://doi.org/10.5194/egusphere-2024-2603
Preprint. Discussion started: 26 August 2024

Kangasluoma, J., Attoui, M., Junninen, H., Lehtipalo, K., Samodurov, A., Korhonen, F., Sarnela, N., Schmidt-Ott, A., Worsnop, D., Kulmala, M., and Petäjä, T.: Sizing of neutral sub 3nm tungsten oxide clusters using Airmodus Particle Size Magnifier, J. Aerosol Sci., 87, 53–62, https://doi.org/10.1016/j.jaerosci.2015.05.007, 2015.

Kangasluoma, J., Samodurov, A., Attoui, M., Franchin, A., Junninen, H., Korhonen, F., Kurtén, T., Vehkamäki, H., Sipilä, M., Lehtipalo, K., Worsnop, D. R., Petäjä, T., and Kulmala, M.: Heterogeneous Nucleation onto Ions and Neutralized Ions: Insights into Sign-Preference, J. Phys. Chem. C, 120, 7444–7450, https://doi.org/10.1021/acs.jpcc.6b01779, 2016a.

Kangasluoma, J., Franchin, A., Duplissy, J., Ahonen, L., Korhonen, F., Attoui, M., Mikkilä, J., Lehtipalo, K., Vanhanen, J., Kulmala, M., and Petäjä, T.: Operation of the Airmodus A11 nano Condensation Nucleus Counter at various inlet pressures and various operation temperatures, and design of a new inlet system, Atmos. Meas. Tech., 9, 2977–2988, https://doi.org/10.5194/amt-9-2977-2016, 2016b.

Kangasluoma, J., Ahonen, L. R., Laurila, T. M., Cai, R., Enroth, J., Mazon, S. B., Korhonen, F., Aalto, P. P., Kulmala, M., Attoui, M., and Petäjä, T.: Laboratory verification of a new high flow differential mobility particle sizer, and field measurements in Hyytiälä, J. Aerosol Sci., 124, 1–9, https://doi.org/10.1016/j.jaerosci.2018.06.009, 2018.

Kangasluoma, J., Cai, R., Jiang, J., Deng, C., Stolzenburg, D., Ahonen, L. R., Chan, T., Fu, Y., Kim, C., Laurila, T. M., Zhou, Y., Dada, L., Sulo, J., Flagan, R. C., Kulmala, M., Petäjä, T., and Lehtipalo, K.: Overview of measurements and current instrumentation for 1–10 nm aerosol particle number size distributions, J. Aerosol Sci., 148, 105584, https://doi.org/10.1016/j.jaerosci.2020.105584, 2020.

Keshavarz, F., Kubečka, J., Attoui, M., Vehkamäki, H., Kurtén, T., and Kangasluoma, J.: Molecular Origin of the Sign Preference of Ion- Induced Heterogeneous Nucleation in a Complex Ionic Liquid–Diethylene Glycol System, J. Phys. Chem. C, 124, 26944–26952, https://doi.org/10.1021/acs.jpcc.0c09481, 2020a.

Keshavarz, F., Kurtén, T., Vehkamäki, H., and Kangasluoma, J.: Seed–Adsorbate Interactions as the Key of Heterogeneous Butanol and Diethylene Glycol Nucleation on Ammonium Bisulfate and Tetramethylammonium Bromide, J. Phys. Chem. A, 124, 10527–10539, https://doi.org/10.1021/acs.jpca.0c08373, 2020b.

Kim, C. S., Okuyama, K., and Fernandez de la Mora, J: Performance Evaluation of an Improved Particle Size Magnifier (PSM) for Single Nanoparticle Detection, Aerosol Sci. Technol., 37, 791–803, https://doi.org/10.1080/02786820300913, 2003.

Kogan, Ya. I. and Burnasheva, Z. A.: Growth and Measurement of Condensation Nuclei in a Continuous Stream, Russian Journal of Physical Chemistry, 34, 1960.

Kulmala, M., Mordas, G., Petäjä, T., Grönholm, T., Aalto, P. P., Vehkamäki, H., Hienola, A. I., Herrmann, E., Sipilä, M., Riipinen, I., Manninen, H. E., Hämeri, K., Stratmann, F., Bilde, M., Winkler, P. M., Birmili, W., and Wagner, P. E.: The condensation particle counter battery (CPCB): A new tool to investigate the activation properties of nanoparticles, J. Aerosol Sci, 38, 289–304, https://doi.org/10.1016/j.jaerosci.2006.11.008, 2007.

Kulmala, M., Kontkanen, J., Junninen, H., Lehtipalo, K., Manninen, H. E., Nieminen, T., Petäjä, T., Sipilä, M., Schobesberger, S., Rantala, P., Franchin, A., Jokinen, T., Järvinen, E., Äijälä, M., Kangasluoma, J., Hakala, J., Aalto, P. P., Paasonen, P., Mikkilä, J., Vanhanen, J., Aalto, J., Hakola, H., Makkonen, U., Ruuskanen, T., Mauldin, R. L., Duplissy, J., Vehkamäki, H.,

https://doi.org/10.5194/egusphere-2024-2603
Preprint. Discussion started: 26 August 2024

Bäck, J., Kortelainen, A., Riipinen, I., Kurtén, T., Johnston, M. V., Smith, J. N., Ehn, M., Mentel, T. F., Lehtinen, K. E. J., Laaksonen, A., Kerminen, V.-M., and Worsnop, D. R.: Direct Observations of Atmospheric Aerosol Nucleation, Science, 339, 943–946, https://doi.org/10.1126/science.1227385, 2013.

Lehtipalo, K., Ahonen, L. R., Baalbaki, R., Sulo, J., Chan, T., Laurila, T., Dada, L., Duplissy, J., Miettinen, E., Vanhanen, J., Kangasluoma, J., Kulmala, M., Petäjä, T., and Jokinen, T.: The standard operating procedure for Airmodus Particle Size Magnifier and nano-Condensation Nucleus Counter, J. Aerosol Sci., 159, 105896, https://doi.org/10.1016/j.jaerosci.2021.105896, 2021.

Li, X., Li, Y., Cai, R., Yan, C., Qiao, X., Guo, Y., Deng, C., Yin, R., Chen, Y., Li, Y., Yao, L., Sarnela, N., Zhang, Y., Petäjä, T., Bianchi, F., Liu, Y., Kulmala, M., Hao, J., Smith, J. N., and Jiang, J.: Insufficient Condensable Organic Vapors Lead to Slow Growth of New Particles in an Urban Environment, Environ. Sci. Technol., 56, 9936–9946, https://doi.org/10.1021/acs.est.2c01566, 2022.

Liu, Y., Attoui, M., Yang, K., Chen, J., Li, Q., and Wang, L.: Size-resolved chemical composition analysis of ions produced by a commercial soft X-ray aerosol neutralizer, J. Aerosol Sci., 147, 105586, https://doi.org/10.1016/j.jaerosci.2020.105586, 2020.

Liu, Y., Attoui, M., Li, Y., Chen, J., Li, Q., and Wang, L.: Factors that govern sub-3 nm particle measurements in an Airmodus® PSM and a TSI ® DEG-SMPS, Aerosol Sci Tech, 1–14, https://doi.org/10.1080/02786826.2022.2098686, 2022.

Liu, Y., Attoui, M., Baalbaki, R., Cai, R., Biskos, G., Chen, Y., and Kangasluoma, J.: Number size distribution and charging properties of sub-10 nm metal-based particles produced by spark ablation at atmospheric pressure, Aerosol Sci. Technol., ahead-of-print, 1–13, https://doi.org/10.1080/02786826.2024.2355174, 2024.

Okuyama, K., Kousaka, Y., and Motouchi, T.: Condensational Growth of Ultrafine Aerosol Particles in a New Particle Size Magnifier, Aerosol Sci. Technol., 3, 353–366, https://doi.org/10.1080/02786828408959024, 1984.

Rönkkö, T., Kuuluvainen, H., Karjalainen, P., Keskinen, J., Hillamo, R., Niemi, J. V., Pirjola, L., Timonen, H. J., Saarikoski, S., Saukko, E., Järvinen, A., Silvennoinen, H., Rostedt, A., Olin, M., Yli-Ojanperä, J., Nousiainen, P., Kousa, A., and Maso, M. D.: Traffic is a major source of atmospheric nanocluster aerosol, Proc. National Acad. Sci., 114, 7549–7554, https://doi.org/10.1073/pnas.1700830114, 2017.

Sgro, L. A. and Fernandez de la Mora, J: A Simple Turbulent Mixing CNC for Charged Particle Detection Down to 1.2 nm, Aerosol Sci. Technol., 38, 1–11, https://doi.org/10.1080/02786820490247560, 2004.

Sulo, J., Enroth, J., Pajunoja, A., Vanhanen, J., Lehtipalo, K., Petäjä, T., and Kulmala, M.: Pushing nano-aerosol measurements towards a new decade – technical note on the Airmodus particle size magnifier 2.0, Aerosol Res., 2, 13–20, https://doi.org/10.5194/ar-2-13-2024, 2024.

Toropainen, A., Kangasluoma, J., Kurtén, T., Vehkamäki, H., Keshavarz, F., and Kubečka, J.: Heterogeneous Nucleation of Butanol on NaCl: A Computational Study of Temperature, Humidity, Seed Charge, and Seed Size Effects, J. Phys. Chem. A, 125, 3025–3036, https://doi.org/10.1021/acs.jpca.0c10972, 2021.

https://doi.org/10.5194/egusphere-2024-2603
Preprint. Discussion started: 26 August 2024

Vanhanen, J., Mikkilä, J., Lehtipalo, K., Sipilä, M., Manninen, H. E., Siivola, E., Petäjä, T., and Kulmala, M.: Particle Size Magnifier for Nano-CN Detection, Aerosol Sci. Technol., 45, 533–542, https://doi.org/10.1080/02786826.2010.547889, 2011.

Wiedensohler, A. and Fissan, H. J.: Bipolar Charge Distributions of Aerosol Particles in High-Purity Argon and Nitrogen, Aerosol Sci. Technol., 14, 358–364, https://doi.org/10.1080/02786829108959498, 1991.

Winkler, P. M., Steiner, G., Vrtala, A., Vehkamäki, H., Noppel, M., Lehtinen, K. E. J., Reischl, G. P., Wagner, P. E., and Kulmala, M.: Heterogeneous Nucleation Experiments Bridging the Scale from Molecular Ion Clusters to Nanoparticles, Science, 319, 1374–1377, https://doi.org/10.1126/science.1149034, 2008.

Wlasits, P. J., Stolzenburg, D., Tauber, C., Brilke, S., Schmitt, S. H., Winkler, P. M., and Wimmer, D.: Counting on chemistry: laboratory evaluation of seed-material-dependent detection efficiencies of ultrafine condensation particle counters, Atmos. Meas. Tech., 13, 3787–3798, https://doi.org/10.5194/amt-13-3787-2020, 2020.

Yao, L., Garmash, O., Bianchi, F., Zheng, J., Yan, C., Kontkanen, J., Junninen, H., Mazon, S. B., Ehn, M., Paasonen, P., Sipilä, M., Wang, M., Wang, X., Xiao, S., Chen, H., Lu, Y., Zhang, B., Wang, D., Fu, Q., Geng, F., Li, L., Wang, H., Qiao, L., Yang, X., Chen, J., Kerminen, V.-M., Petäjä, T., Worsnop, D. R., Kulmala, M., and Wang, L.: Atmospheric new particle formation from sulfuric acid and amines in a Chinese megacity, Science, 361, 278–281, https://doi.org/10.1126/science.aao4839, 2018.